JOURNAL OF GEOPHYSICAL RESEARCH, VOL. 104, NO. D24, PAGES 31,333–31,349, DECEMBER 27, 1999

Wavelength dependence of the optical depth of biomass burning, urban, and desert dust aerosols

T. F. Eck,[1] B. N. Holben,[2] J. S. Reid,[3] O. Dubovik,[4] A. Smirnov,[4] N. T. O'Neill,[5] I. Slutsker,[4] and S. Kinne[6]

Abstract. The Angstrom wavelength exponent α, which is the slope of the logarithm of aerosol optical depth (τ_a) versus the logarithm of wavelength (λ), is commonly used to characterize the wavelength dependence of τ_a and to provide some basic information on the aerosol size distribution. This parameter is frequently computed from the spectral measurements of both ground-based sunphotometers and from satellite and aircraft remote sensing retrievals. However, spectral variation of α is typically not considered in the analysis and comparison of values from different techniques. We analyze the spectral measurements of τ_a from 340 to 1020 nm obtained from ground-based Aerosol Robotic Network radiometers located in various locations where either biomass burning, urban, or desert dust aerosols are prevalent. Aerosol size distribution retrievals obtained from combined solar extinction and sky radiance measurements are also utilized in the analysis. These data show that there is significant curvature in the ln τ_a versus ln λ relationship for aerosol size distributions dominated by accumulation mode aerosols (biomass burning and urban). Mie theory calculations of α for biomass burning smoke (for a case of aged smoke at high optical depth) agree well with observations, confirming that large spectral variations in α are due to the dominance of accumulation mode aerosols. A second order polynomial fit to the ln τ_a versus ln λ data provides excellent agreement with differences in τ_a of the order of the uncertainty in the measurements (~0.01-0.02). The significant curvature in ln τ_a versus ln λ for high optical depth accumulation mode dominated aerosols results in α values differing by a factor of 3-5 from 340 to 870 nm. We characterize the curvature in ln τ_a versus ln λ by the second derivative α' and suggest that this parameter be utilized in conjunction with α to characterize the spectral dependence of τ_a. The second derivative of ln τ_a versus ln λ gives an indication of the relative influence of accumulation mode versus coarse mode particles on optical properties.

1. Introduction

Variability in the size distribution of atmospheric aerosols results in part from variability in the processes that initially form the aerosols such as biomass burning [*Reid and Hobbs*, 1998; *Remer et al.*, 1998], combustion of fossil fuels from urban/industrial processes [*Remer and Kaufman*, 1998], oceanic wave action producing sea salt aerosol [*Hoppel et al.*, 1990], plants producing biogenic aerosols [*Kavouras et al.*, 1998; *Artaxo et al.*, 1988], volcanic eruptions [*Russell et al.*, 1993] and airborne soil particles [*d'Almeida*, 1987]. In addition, once these aerosols have been formed there are often dynamic processes that may result in evolution of the size distribution in time. For example, in the case of biomass burning aerosols, *Reid et al.* [1998] show that aging of the aerosols results in changes in aerosol size distribution related to coagulation, condensation, and gas-to-particle conversion processes. Similarly *Remer and Kaufman* [1998] have observed variability in the size distributions of urban/industrial aerosols which are likely due to particle growth at high relative humidity and aerosol interactions with clouds.

These variations in size distribution of various aerosol types strongly influence the radiative properties of the aerosols such as the scattering phase function, single scattering albedo, and spectral variation of aerosol optical thickness. The characterization of the spectral dependence of aerosol optical thickness τ_a in the atmosphere is important for modeling of the radiative effects of aerosols on the atmosphere/surface system, retrieval of aerosol parameters from satellite remote sensing, correction for aerosol effects in remote sensing of the Earth's surface, and assistance in identification of aerosol source regions and aerosol evolution in time. Many studies of aerosol optical thickness and its spectral dependence rely on the Angstrom wavelength exponent α to quantify this spectral dependence. *Angstrom's* [1929] empirical expression is given as

$$\tau_a = \beta\lambda^{-\alpha} \quad (1)$$

where λ is the wavelength in microns of the corresponding τ_a

[1]Raytheon ITSS, NASA Goddard Space Flight Center, Greenbelt, Maryland
[2]Biospheric Sciences Branch, NASA Goddard Space Flight Center, Greenbelt, Maryland
[3]Tropospheric Branch, Space and Naval Warfare Systems Center, San Diego, California.
[4]Science Systems Applications, Inc., NASA Goddard Space Flight Center, Greenbelt, Maryland
[5]Centre d'Applications et de Recherches en Teledetetection, Universite de Sherbrooke, Quebec; currently on leave at NASA Goddard Space Flight Center, Greenbelt, Maryland
[6]University of Maryland, Baltimore, Maryland and NASA Goddard Space Flight Center, Greenbelt, Maryland

Paper number 1999JD900923.
0148-0227/99/1999JD900923$09.00

values and β is Angstrom's turbidity coefficient which equals τ_a at λ=1 μm. By ratioing equation (1) at two different wavelengths and then taking the logarithm the Angstrom wavelength exponent may be computed from spectral values of τ_a by

$$\alpha = -\frac{d\ln\tau_a}{d\ln\lambda} = -\frac{\ln\left(\frac{\tau_{a_2}}{\tau_{a_1}}\right)}{\ln\left(\frac{\lambda_2}{\lambda_1}\right)}, \quad (2)$$

and therefore α as defined in (2) is the negative of the slope (or negative of the first derivative) of τ_a with wavelength in logarithmic scale. Typical values of α range from >2.0 for fresh smoke particles, which are dominated by accumulation mode aerosols [*Kaufman et al.*, 1992] to nearly zero for high optical thickness Sahelian/Saharan desert dust cases dominated by coarse mode aerosols [*Holben et al.*, 1991]. *O'Neill and Royer* [1993] analyzed α computed from five visible and near infrared wavelengths (380-862 nm), and found a relationship between the effective radius of the number size distribution and the value of α.

The Angstrom wavelength exponent is related to the Junge or power law size distribution [*Junge*, 1955] by α=v–2, where

$$\frac{dN}{d\ln r} = cr^{-v} \quad (3)$$

is the differential number density for which the radius r extends from zero to infinity. However, as noted by *King and Byrne* [1976] the size distributions of aerosols typically do not follow the Junge distribution nor have radii extending from zero to infinity, and that departure from these conditions often introduces curvature in the ln τ_a versus ln λ relationship. Therefore they utilized a second-order polynomial fit of the form

$$\ln\tau_a = a_0 + a_1\ln\lambda + a_2(\ln\lambda)^2 \quad (4)$$

to account for the curvature in ln τ_a versus ln λ. *Kaufman* [1993] analyzed the spectral dependence of τ_a from sunphotometer measurements and found that values of α often vary for computations made from different wavelength intervals due to the departure of the aerosol size distribution from a power law.

In addition to the aerosol size distribution influencing the spectral dependence of τ_a, the magnitude of the aerosol absorption and its spectral dependence are also factors that need to be considered. The total extinction aerosol optical depth $\tau_a = \tau_{ext}$ can be described as:

$$\tau_a = \tau_{ext} = \tau_{sct} + \tau_{abs} \quad (5)$$

where τ_{sct} is the scattering optical depth and τ_{abs} is the absorption optical depth. The aerosol single scattering albedo, ω_0, can be determined for a given wavelength by:

$$\omega_0 = \frac{\tau_{sct}}{\tau_{ext}} \quad (6)$$

Spectral variation of single scattering albedo in the visible and near infrared has been inferred for biomass burning aerosols [*Eck et al.*, 1998; *Dubovik et al.*, 1999] and computed or inferred for desert dust [*d'Almeida*, 1987; *Tegen and Lacis*, 1996; *Kaufman et al.*, 1999]. Spectrally varying values of ω_0 range from ~0.70 to 0.92 for biomass burning aerosols and from ~0.70 to 0.99 for desert dust. Therefore, while the spectral dependence of total or extinction aerosol optical depth is dominated by scattering effects, variability in absorption can be an important term.

Recent studies have shown useful applications of α measurements for characterization of aerosol physical and radiative properties. *Reid et al.* [1999] have shown that α, computed from sunphotometer measured values of τ_a, show significant spectral variation for biomass burning smoke measured in Brazil. They have shown that α computed from shorter wavelength pairs (i.e. 340 and 440 nm or 440 and 670 nm) has much greater sensitivity to accumulation mode aerosol particle size (measured in situ from aircraft) than does α computed from longer wavelength measurements of τ_a. *Nakajima and Higurashi* [1998] retrieved α from satellite measurements and demonstrated how these techniques differentiate, on a global scale, the differences between accumulation mode-dominated aerosols (urban and biomass burning) and coarse-particle aerosols (desert dust).

In this paper we investigate the spectral variations of aerosol optical thickness as measured by ground-based sunphotometry from several instruments in the Aerosol Robotic Network (AERONET) globally distributed network [*Holben et al.*, 1998]. We focus on the variability in τ_a spectral dependence for three major and distinct aerosol types: biomass burning aerosols in South America and Africa, urban/industrial from the east coast of the United States, and desert dust from Asia and the Middle East. Aerosol volume size distributions retrieved from combined solar extinction and almucantar sky radiance measurements are also utilized for all the aerosol types studied in this analysis.

2. Instrumentation and Methods

All of the measurements reported in this paper were made with Sun-sky radiometers, which are a part of the AERONET global network. These instruments are described in detail by *Holben et al.* [1998]; however, a brief description will be given here. The automatic tracking Sun and sky scanning radiometers made direct Sun measurements with a 1.2° full field of view every 15 min at 340, 380, 440, 500, 675, 870, 940, and 1020 nm (nominal wavelengths). The direct Sun measurements take 8 s to scan all 8 wavelengths, with a motor-driven filter wheel positioning each filter in front of the detector. These solar extinction measurements are then used to compute aerosol optical depth at each wavelength except for the 940 nm channel, which is used to retrieve total precipitable water in centimeters. The filters utilized in these instruments were ion-assisted deposition interference filters with band pass (full width at half maximum) of the 340 nm channel at 2 nm and the 380 nm filter at 4 nm, while the band pass of all other channels was 10 nm. The AERONET data we present here were quality- and cloud-screened following the methodology of A. Smirnov et al. (Cloud screening and quality control algorithms for the AERONET data base, submitted to *Remote Sensing of Environment*, 1999).

The sky radiance almucantar measurements at 440, 675, 870, and 1020 nm in conjunction with the direct Sun measured τ_a at these same wavelengths were used to retrieve aerosol size distributions following the methodology of *Dubovik et al.* [1999]. Almucantar sky radiance measurements were made at

optical airmasses of 4, 3, and 2 in the morning and afternoon, and once per hour in between. Sensitivity studies performed by O. Dubovik et al. (Accuracy assessments of aerosol optical properties retrieved from AERONET Sun and sky radiance measurements, submitted to *Journal of Geophysical Research*, 1999, hereinafter referred to as Dubovik et al., submitted manuscript, 1999) analyzed the perturbations of the inversion resulting from random errors, possible instrument offsets, and known uncertainties in the atmospheric radiation model. Retrieval tests using known size distributions demonstrated successful retrievals of mode radii and the relative magnitude of modes for various types of size distributions such as bimodal accumulation mode-dominated aerosols and bimodal coarse mode-dominated aerosols.

The data that we analyzed for the Goddard Space Flight Center (GSFC) in Maryland utilized only τ_a measurements from Mauna Loa Observatory (MLO) calibrated instruments. These reference instruments are typically recalibrated at MLO every 2-3 months using the Langley plot technique. The zero air mass voltages (V_0, instrument voltage for direct normal solar flux extrapolated to the top of the atmosphere [*Shaw*, 1983]) are inferred to an accuracy of ~0.2-0.5% for the MLO calibrated reference instruments [*Holben et al.*, 1998]. Therefore the uncertainty in τ_a due to the uncertainty in zero airmass voltages for the reference instruments is better than 0.002-0.005. The Sun-sky radiometers at sites other than GSFC utilized in this study were intercalibrated against a MLO calibrated AERONET reference instrument both before deployment in the field and post deployment. A linear rate of change in time of the zero airmass voltages is then assumed in the processing of the data from field sites. Our analysis suggests that this results in an uncertainty of ~0.01–0.02 in τ_a (wavelength dependent) because of calibration uncertainty for the field instruments.

In the computation of τ_a from the direct Sun measurements the Rayleigh optical depth is subtracted out from the total optical depth. We compute the Rayleigh optical depth from the equation of *Penndorf* [1957], utilizing the refractive index of air given by *Elden* [1966], and the depolarization factor given by *Young* [1980]. However, since atmospheric pressure is not measured, there is no adjustment of Rayleigh optical depth for departure from mean surface pressure. This may result in an additional error in computed τ_a which would be the largest for the short wavelengths with high Rayleigh optical depth. Therefore, at 340 nm the maximum error in computed τ_a due to atmospheric pressure variations (assuming a 3% maximum departure from mean surface pressure) is ~0.021, while at 380 nm the error would be 0.013, at 440 nm it would be 0.007, and at 1020 nm it would be 0.0002. These are maximum errors; typical errors due to surface pressure variability would be less than one half the magnitude of these maxima. These errors would also have a strong tendency to be biased in one direction since low pressure results in extensive cloud cover and thus very few direct Sun observations. Additionally, in the computation of τ_a for 340, 500, and 675 nm, ozone optical depth is also subtracted from total optical depth using climatological mean ozone values from *London et al.* [1976]. Departures from these climatological values by 50% (which are very large fluctuations) would result in additional uncertainty in computed τ_a of only ~0.0036 at 340 nm, 0.0045 at 500 nm, and 0.0063 at 675 nm. Again, these are the probable maximum departures due to total column ozone variability, and typical departures would be less than half this magnitude. We compute the combination of calibration uncertainties of V_0 and uncertainty in ozone and Rayleigh optical depth, for optical airmass of 1, in the manner of *Russell et al.* [1993]. For our computation we assume that the uncertainties in Rayleigh and ozone optical depths are equal to one third of the maximum values given above. We therefore calculate an estimated total uncertainty of ~0.010-0.021 in computed τ_a for field instruments (which is spectrally dependent with the higher errors in the UV) and ~0.002-0.009 for reference instruments. *Schmid et al.* [1999] compared τ_a values derived from four different solar radiometers (one was an AERONET Sun-sky radiometer) operating simultaneously together in a field campaign and found that the τ_a values from 380 to 1020 nm agreed to within 0.015 (rms), which is similar to our estimated level of uncertainty in τ_a retrieval for field instruments.

The effect of the forward scattered diffuse radiation within the 1.2^0 full field of view of the sunphotometer has also been considered [*Box and Deepak*, 1979; *Halthore et al.*, 1997]. The magnitude of the diffuse radiation effect within the field of view of the instrument is dependent on the aerosol size distribution that may be parameterized by the effective radius. The effective radius (r_{eff}) is defined by *Hansen and Travis* [1974] as

$$r_{\text{eff}} = \frac{\int_0^\infty \pi r^3 \frac{dN}{dr} dr}{\int_0^\infty \pi r^2 \frac{dN}{dr} dr} \tag{7}$$

where N is the total columnar number density and r is the particle radius.

Simulations by *Kinne et al.* [1997] show that for aerosol particles with effective radius of 0.2 μm, there is essentially no effect on measured aerosol optical depth, even for sunphotometers with a 2^0 full field of view. This effective radius is of the same order of magnitude as that for smoke or urban/industrial aerosols. For desert dust particles with an effective radius of 1.75 μm (similar to a dust case presented later in the paper) the computed apparent optical depth from the sunphotometer measurements in the absence of forward scattered diffuse radiation correction would be ~0.7% lower than the actual optical depth.

3. Data and Analysis of Spectral τ_a Variability

In this section we present the measurements of spectral τ_a from 340 to 1020 nm for three distinct aerosol types. The nature and causes of the spectral variability are discussed and related to features in the aerosol size distribution.

3.1. Biomass Burning Aerosols

Extensive biomass burning associated with agricultural practices occurs during the latter half of the dry season (August-September) across large portions of the southern and eastern Amazon Basin each year [*Prins and Menzel*, 1994]. This burning produces large amounts of smoke aerosol with high optical depth, especially during the peak burning season months of August through September [*Holben et al.*, 1996].

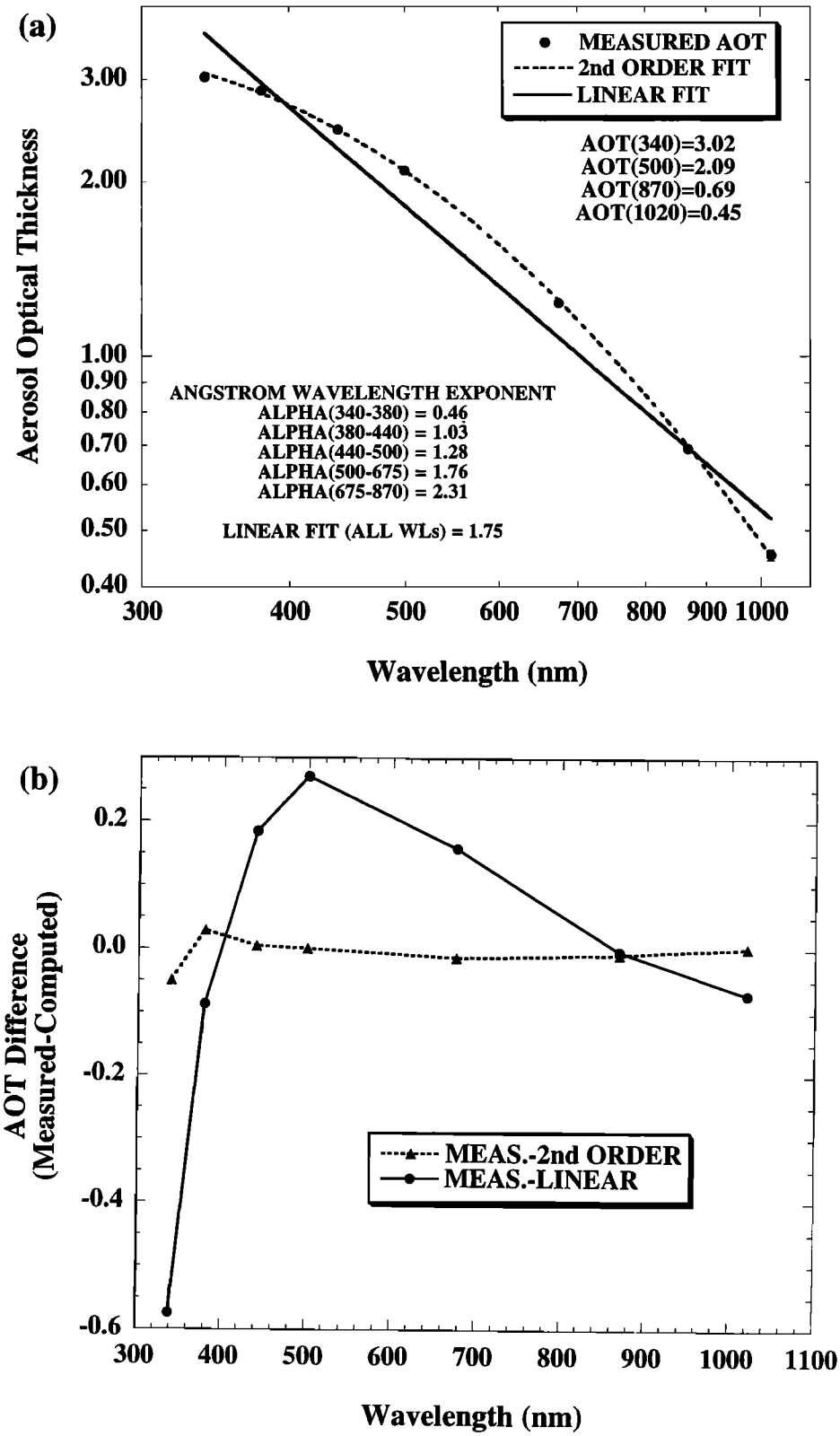

Figure 1. (a) The spectral variation of measured τ_a (340-1020 nm) from an Aerosol Robotic Network (AERONET) CIMEL radiometer for biomass burning aerosols in Concepcion, Bolivia, on August 24, 1998, at 1541 UT. The linear fit and the second-order polynomial fit of ln τ_a versus ln λ to the measurements are also shown. The aerosol optical thickness (AOT) for this case at 500 nm was 2.09. The uncertainty in τ_a is also plotted as error bars, but it is smaller than the symbol size except at 1020 nm. (b) The difference between the measured τ_a (shown in Figure 1a) and the value obtained from the linear and second-order polynomial fits at the measurement wavelengths.

Here we present the AERONET data from two locations in the Bolivian Amazon Basin, both downwind from major regions of biomass burning. We also present some measurements of biomass burning aerosols made in Mongu, Zambia (15°15'S, 23°09'E), in order to show a comparison of smoke optical properties between some African and South American sites. Mongu is located in a savanna region, which is a mix of open woodland and grassland, which is seasonally burned at the end of the dry season (August-November).

The first site in South America, Concepcion, Bolivia (16°08'S, 62°01'W), is in a region consisting of mixed agriculture and tropical forest, with some local biomass burning and downwind from major sources of smoke in Bolivia and Brazil. Figure 1a shows the measured wavelength dependence of the biomass burning τ_a for a nearly instantaneous measurement made on August 24, 1998, at 1541 UT (solar zenith=28.1°). The τ_a was high on this date and time with a value of 2.09 at 500 nm and ranged from 3.02 at 340 nm to 0.45 at 1020 nm. The data show a pronounced curvature of τ_a versus λ on the logarithmic scale, with a second-order polynomial curve (equation (4)) providing an excellent fit to the measured data. The linear Angstrom-type regression fit to all wavelengths, also shown in Figure 1a, demonstrates how large departures from the measurement values at some wavelengths can occur for the first-order Angstrom fit. Figure 1b shows the difference between the measured τ_a and the values from the linear and second-order polynomial fits of ln τ_a versus ln λ. The differences between measured τ_a and second order polynomial fit values were 0.05 or less, with differences of 0.014 or less for the wavelengths of 440-1020 nm. In contrast, the differences in τ_a for the linear fit ranged from –0.57 at 340 nm to +0.27 at 500 nm. As a result of the curvature in ln τ_a versus ln λ, the Angstrom exponent computed for adjacent wavelength pairs (equation (2)) varies from 0.46 for the 340-380 nm wavelength pair to 2.31 for the 675-870 nm pair, or approximately a factor of 5 in magnitude over this wavelength range. The linear fit to all wavelengths yields an Angstrom wavelength exponent of 1.75 for this case.

In order to investigate the reason for the curvature in ln τ_a versus ln λ we compare the α values for biomass burning aerosols computed from Mie theory to measurements made with AERONET radiometers. *Martins et al.* [1998] made measurements of particle shape in smoke hazes in Amazonia and found that the particles in regional hazes were largely spherical, thus validating the use of spherical particle Mie calculations. The volume size distribution used as input to the Mie calculations was measured in situ by a differential mobility particle sizer (DMPS) on the UW C-131A aircraft [*Reid et al.*, 1998] during the Smoke, Clouds, and Radiation-Brazil (SCAR-B) experiment in Brazil in August-September 1995. The volume size distribution, for the accumulation mode particles only (<0.6 μm), was parameterized by a lognormal distribution fit with a volume median radius of 0.175 μm and a

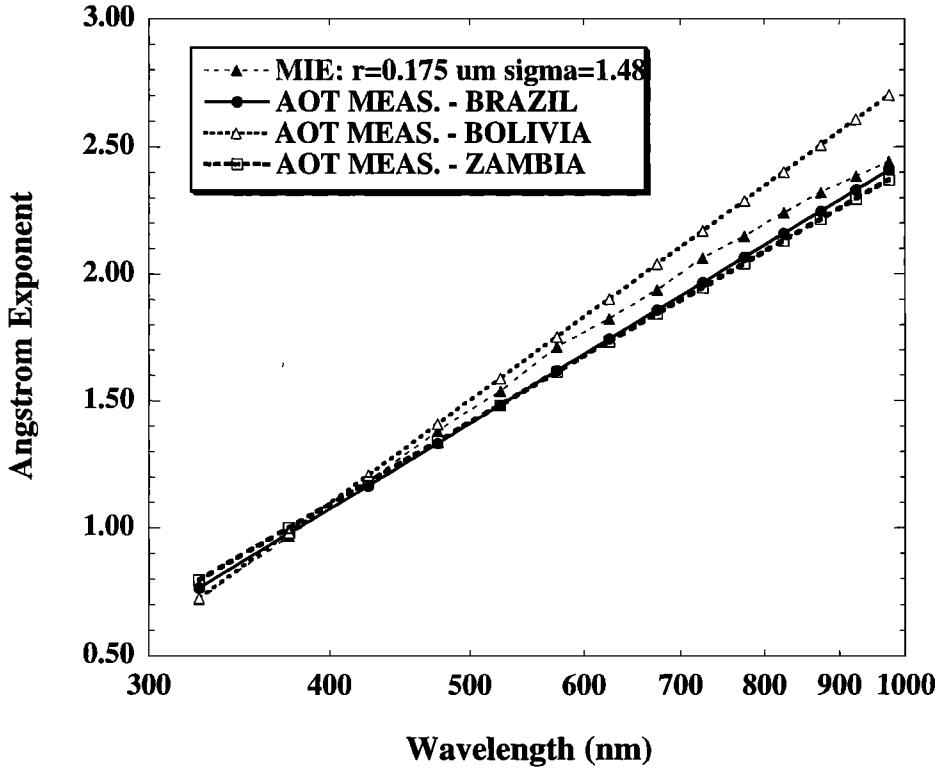

Figure 2. Comparison of the spectral variation of the Angstrom exponent α versus wavelength for Mie computed values and measurements for biomass burning aerosols. Mie computations utilize aircraft measured aerosol size distributions from the differential mobility particle sizer (DMPS) instrument during the Smoke, Cloud, and Radiation-Brazil (SCAR-B) experiment in 1995. Measurements of τ_a were made in Mongu, Zambia on September 1, 1997, in Rondonia, Brazil on September 6, 1995, and in Concepcion, Bolivia on August 24, 1998. Values of τ_a were determined by second-order polynomial fit to the measurements and then used to compute α at 50 nm intervals. Data for both the measured size distribution and measured τ_a are representative of well-aged smoke aerosols.

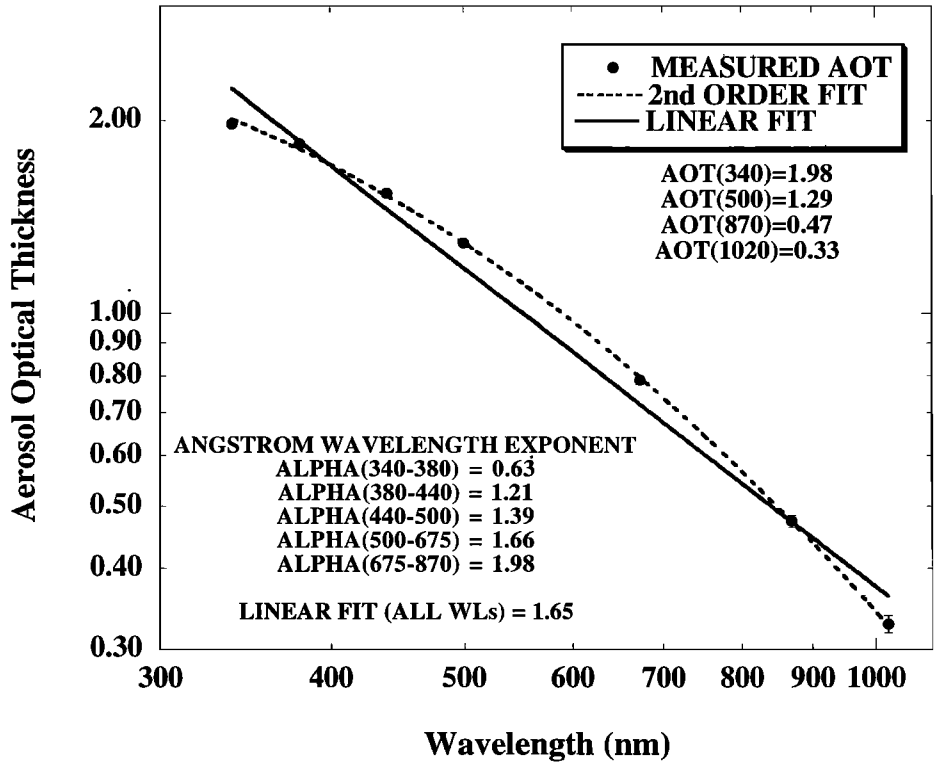

Figure 3. Same as Figure 1a except for biomass burning aerosols in Mongu, Zambia on September 1, 1997 at 0858 UT with $\tau_{a500} = 1.29$.

geometric standard deviation of 1.48 (values representative of aged smoke in central Brazil (Cuiaba)). The particles were modeled as layered spheres with a black carbon core comprising 6% of the mass (refractive index: m=1.8-0.6i) and a non absorbing shell (m=1.5-0i). This aerosol optical configuration produces absorption levels (single scattering albedo) typical of measurements made by several in situ (aircraft-based) techniques during SCAR-B [*Reid et al.*, 1998]. In Figure 2 the Mie computed values of α are computed for 50 nm wavelength ranges from values of the computed spectral extinction coefficients. The measured values of α are computed for these same wavelength ranges from the second-order polynomial curve fit to the measured values of τ_a. Measurements of biomass burning aerosols shown in Figure 2 are from AERONET instruments located in Rondonia, Brazil (Potosi Mine), during SCAR-B (September 6, 1995; τ_{a500}=2.03), in Mongu, Zambia (September 1, 1997; τ_{a500}=1.29), and in Concepcion, Bolivia (August 24, 1998; τ_{a500}=2.09 (see Figure 1)). For all three of these cases the measured aerosol optical depths are high for their respective regions during their peak burning seasons and therefore are likely to have a significant percentage of well-aged aerosol, which may be similar to the size distribution selected for input to the Mie computations. Burning in these regions occurs with numerous small local fires and with smoke levels sometimes building over several days or with dense smoke being advected from other burning regions, therefore aged aerosols are likely to be present. As is seen in Figure 2, there is excellent agreement (within 0.1 or less) between the Mie computed and measured values of α for biomass burning aerosols for the Brazil and Zambia cases and to within 0.25 or less for the Bolivian case. This confirms that a size distribution dominated by accumulation mode aerosols results in a second-order ln τ_a versus ln λ curvature. Differences in the wavelength dependence of α between the measurement sites on these dates and to the Mie calculations may be due to a variety of factors. These factors include differences in the volume median radius of the accumulation mode aerosols, the geometric standard deviation of the mode, the magnitude of a coarse-aerosol mode (which is not included in the Mie calculations), and the spectral variation of ω_o. This analysis, along with the data from Mongu, Zambia, presented in Figure 3 and Table 1 shows that the wavelength dependence of optical depth for well-aged biomass burning aerosols is similar for South American and African source regions. However, it is emphasized that there is significant variability in accumulation mode size distributions for smoke aerosols due to several processes being associated with the aging [*Reid et al.*, 1998] and that the data presented in Figure 2 are representative of only well-aged biomass burning aerosols at high concentrations.

The aerosol volume size distribution, dV/d (ln r), as derived from analysis of the combined extinction and almucantar sky radiances [*Dubovik et al.*, 1999, also submitted manuscript, 1999] for the Concepcion, Bolivia, August 24, 1998 case (Figure 1) is shown in Figure 4. All size distributions presented and discussed in this paper are volume size distributions. (Note that the time of day of the almucantar measurements may differ from the times of the τ_a data presented, resulting, in some cases, in differences in τ_a for the two observation times; for example see Table 1 and Figure 4.) The size distribution in Figure 4 shows that the accumulation

Table 1. Angstrom Exponent (α) Computed for Several Wavelength Pairs and From Regression to All Wavelengths and the Negative of the Second Derivative α' for Instantaneous τ_a Observations Made at Several Sites With Differing Aerosol Types

Site	Aerosol Type	Date Time	AOT 500 nm	α All λ	α (380-440)	α (440-675)	α (675-870)	α'
Concepcion, Bolivia	biomass burning	July 28, 1998 1414 UT	0.23	1.98	1.90	1.78	2.38	+0.75
Concepcion, Bolivia	biomass burning	Aug. 2,1998 1530 UT	0.57	1.85	1.48	1.70	2.30	+1.31
Concepcion, Bolivia	biomass burning	Aug. 24,1998 1541 UT	2.09	1.75	1.03	1.61	2.31	+2.09
Mongu, Zambia	biomass burning	Sept. 01,1997 0858 UT	1.29	1.65	1.21	1.58	1.98	+1.24
GSFC	urban/ industrial	July 15, 1997 1458 UT	1.02	1.65	1.01	1.55	2.15	+1.76
GSFC	urban/ industrial	June 25, 1997 1233 UT	0.38	1.79	1.45	1.82	2.09	+1.10
GSFC	urban/ industrial	May 15,1998 1241 UT	0.17	1.57	1.79	1.79	1.38	-0.22
Dalanzadgad, Mongolia	desert dust	April 18, 1998 1008 UT	0.44	0.19	0.31	0.21	0.07	-0.20
Bahrain	desert dust + [a]	Aug 5, 1998 1144 UT	0.41	1.00	1.35	1.06	0.99	-0.11

AOT, aerosol optical thickness; GSFC, Goddard Space Flight Center, Greenbelt, Maryland.

[a]Aerosol with coarse mode desert dust plus an accumulation mode (see Figure 13).

mode particles (< 0.6 μm) dominate for this case, with the integrated volume of this mode being nearly an order of magnitude greater than the coarse particle mode. One can also observe that the accumulation mode size distribution for August 24, 1998, in Concepcion appears to be nearly lognormally distributed. Also shown in Figure 4 is the retrieved aerosol size distributions for two more cases at Concepcion in 1998 when τ_a was lower than on August 24. It is further noted for the August 2 (τ_{a500}=0.58) and July 28 (τ_{a500}=0.29) inversions that the magnitude of the accumulation mode decreases substantially when the aerosol optical thickness decreases, yet the change in the magnitude of the coarse mode is not always as great. Therefore the relative magnitude of the accumulation versus coarse modes changes as aerosol optical depth changes. This results in a change of the curvature of the ln τ_a versus ln λ relationship and also in a change in the Angstrom wavelength exponent.

As a parameter to quantify the curvature of the ln τ_a versus ln λ relationship we utilize the second derivative of ln τ_a versus ln λ or the derivative of α with respect to the logarithm of wavelength. The second derivative is a measure of the rate of change of the slope with respect to wavelength and therefore is a logical complement to the Angstrom exponent, which is the negative of the slope (first derivative) of ln τ_a versus ln λ. We use the following approximation to compute the second derivative [*Li et al.*, 1993], and we define $\alpha'(\lambda_i)$ at wavelength λ as the negative of the second derivative (since α is defined as the negative of the first derivative):

$$\alpha'(\lambda_i)=\frac{d\alpha}{d\ln\lambda}=-\left(\frac{2}{\ln\lambda_{i+1}-\ln\lambda_{i-1}}\right)\left(\frac{\ln\tau_{a_{i+1}}-\ln\tau_{a_i}}{\ln\lambda_{i+1}-\ln\lambda_i}-\frac{\ln\tau_{a_i}-\ln\tau_{a_{i-1}}}{\ln\lambda_i-\ln\lambda_{i-1}}\right). \quad (8)$$

We compute the second derivative of ln τ_a versus ln λ using the wavelengths 380, 500, and 870 nm (Table 1). It is noted that the second derivative can also be computed by second-order polynomial curve fit to all wavelengths of τ_a data and that a minimum of three wavelengths is required. In Table 1 it is seen that the negative value of the second derivative computed for these wavelengths increases as τ_a increases for the three Concepcion dates presented. This is to be expected since the curvature is greater as the influence of the accumulation mode versus coarse mode increases [*Kaufman*, 1993]. Also note (Table 1) that the value of α computed from the 675-870 nm wavelength pair changes very little (~3% relative change), while the value of α computed from the 380-440 nm wavelength pair changes significantly, by ~46%. Examination of Figure 4 reveals that as the magnitude of the accumulation mode peak increases (with increasing τ_a), the modal peak radius also increases in size for these three cases. *Reid et al.* [1998] have shown that this is likely to be due to the aging processes of biomass burning aerosols, whereby the particle size increases with time because of both coagulation- and diffusion-limited processes (e.g., condensation, gas-to-

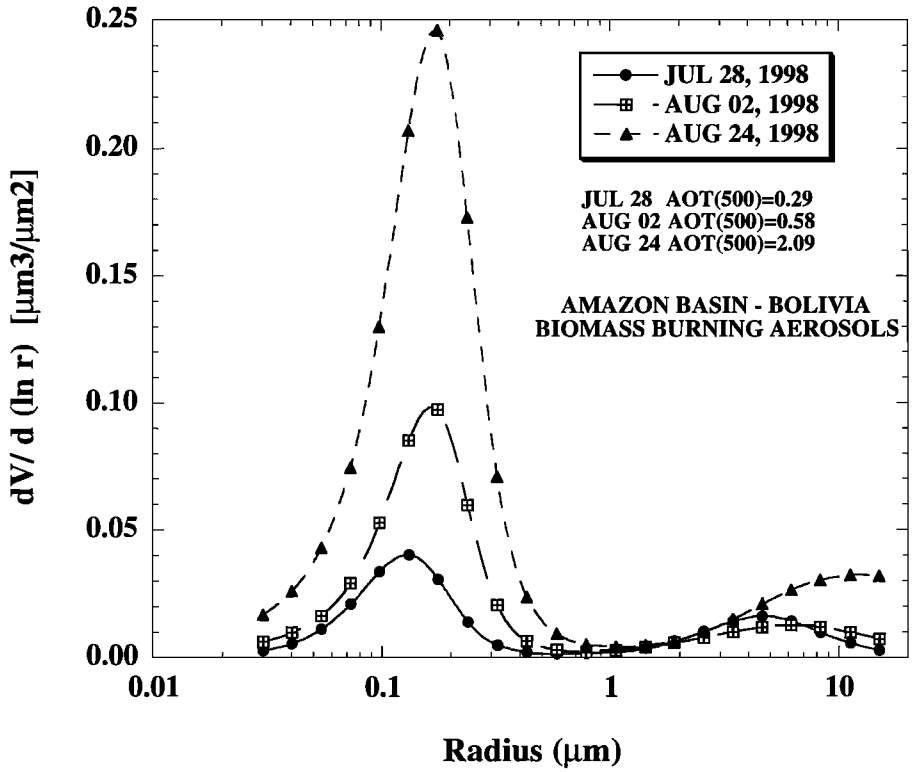

Figure 4. Aerosol volume size distributions for biomass burning aerosols in Concepcion, Bolivia, for 3 days in July-August 1998 with different aerosol optical depths. Aerosol size distribution retrievals were derived from simultaneous analysis of sky radiances in the almucantar and spectral τ_a at 440, 675, 870, and 1020 nm. The retrievals were derived from observations made at 1816 UT on July 28, at 1716 UT on August 02, and at 1713 UT on August 24, 1998.

particle conversion, and some cloud processes). *Reid et al.* [1999] have found that for biomass burning aerosols in Brazil the Angstrom exponent from short wavelength pairs (340-440 and 440-670 nm) is highly correlated (r^2>0.79) with volume median diameter of the accumulation mode, while α from long wavelength pairs (500-870 and 670-1020 nm) are very weakly correlated (r^2<0.10) with particle volume median diameter. This results from both a narrowing of the size distribution and a growth in particle size as these biomass burning particles evolve with age [*Reid et al.*, 1998]. We also present the values of the Angstrom exponent for the 440-675 nm wavelength pair in Table 1 since retrievals of τ_a will be made over land surfaces at these wavelengths from the Moderate-resolution Imaging Spectroradiometer (MODIS) sensor on the Terra satellite to be launched in 1999. It is noted that the 440-675 nm α values for Concepcion show a response to changes in the aerosol volume size distribution, although with less sensitivity than the 380-440 wavelength pair value of α.

We examined the seasonal variation of the spectral wavelength dependence of biomass burning smoke at another AERONET site in Bolivia. Los Fierros, Bolivia (14°33'S, 60°55'W), is located within Noel Kempff Mercado National Park in central eastern Bolivia. In this region, there is very little biomass burning since there is essentially no burning in the park and a minimum of agricultural activity and/or burning in a large area to the west of the site, where the land is designated forest and wildlife reserves. The total size of this protected region is ~300 by 130 km with minimal fire activity as detected from satellite [*Prins et al.*, 1998]. However, there is very extensive biomass burning surrounding this region in all directions, with particularly heavy burning and smoke production from Rondonia, Brazil, to the north and from northern Bolivia and the Beni grasslands region (to the west). The smoke from these various regions is advected over the site as the air parcel trajectories change, and the age of the smoke varies as a function of distance from source regions and speed of the wind.

The increase of τ_a with time from May 4 through Sepember 1, 1998, is quite dramatic (Figure 5), with τ_a at 500 nm often below 0.15 in magnitude through mid-June (since there was very little burning in this time period) and then beginning a steady increase as fire activity increased, to maximum values above 3.0. The seasonal variation of the α values computed from the linear regression fit of the 440, 500, 675, and 870 nm τ_a data is shown in Figure 6a, while the seasonal variation of the second derivative (computed from the second-degree polynomial fit to the 380, 440, 500, and 870 nm τ_a data) is shown in Figure 6b. The α values show a general increasing trend from May to August as the fine-particle smoke aerosols become more dominant. The low α values in May (0.4-1.5) may be influenced by large particles that are biogenically produced over the tropical forest, as large particles were found over Brazilian rainforest in the wet season during the Large Scale Biosphere-Atmosphere Experiment in Amazonia - Cooperative LBA Airborne Regional Experiment (LBA-CLAIRE) experiment [*Artaxo et al.*, 1998]. It is noted that at

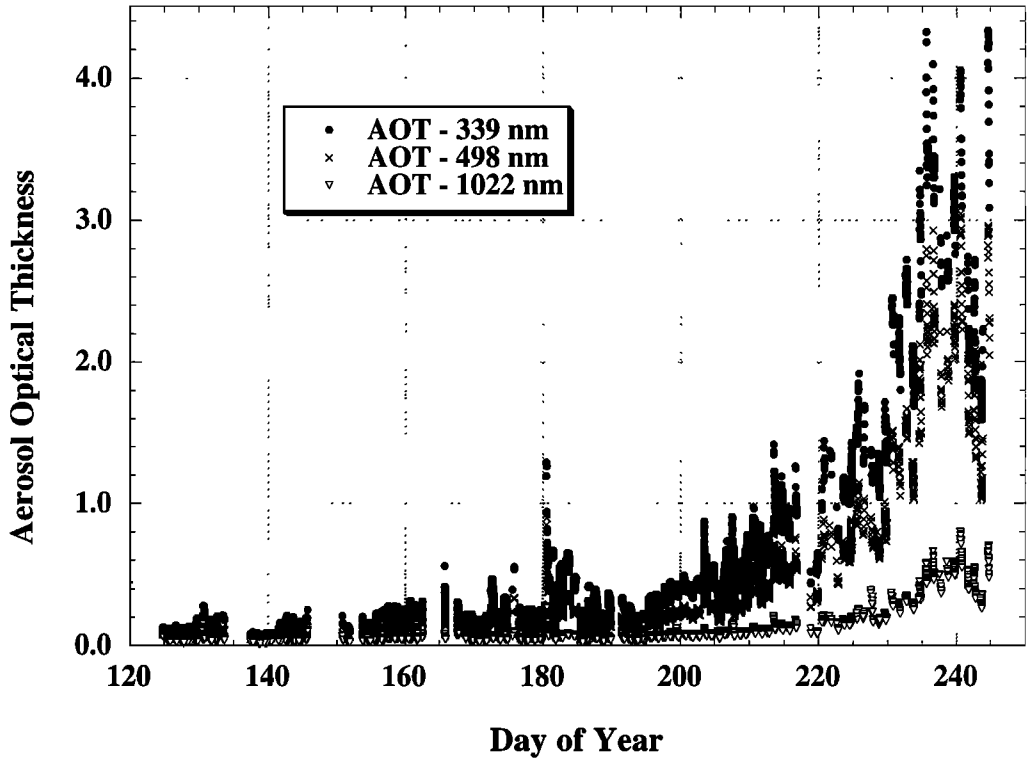

Figure 5. The seasonal variation of τ_a at 339, 498, and 1022 nm at Los Fierros, Bolivia from May 4 through September 1, 1998, showing preburning season values in May and peak burning season values in middle-late August.

about day 181, there is a sharp isolated increase in τ_a (Figure 5) that shows a corresponding large increase in α due to the passage of a plume of relatively fresh smoke over the site. This event resulted in the largest values in α of the entire season and also some of the highest values of α' (Figure 6b). The seasonal values of α' (Figure 6b), show a tendency toward increasing values as the season progresses and τ_a increases. The relationship between α and τ_a for the entire season (Figure 7a) shows that there is a strong tendency for α to increase as τ_{a500} increases from 0.05 to 0.25 as the aerosol optical depth moves from background dominated to biomass burning dominated. When τ_a is higher than 0.25 there is a leveling off of α as τ_a increases further but with 2 or 3 populations of values ranging from 1.6 to 2.1. The differences in α at large τ_a are likely to be due to the variation in particle size as a result of the aging of the biomass burning aerosols [*Reid et al.*, 1999] and the conditions under which the aerosols were produced, such as whether the production was primarily from flaming phase or smoldering phase combustion. The relationship between α' and τ_a for the entire season (Figure 7b) shows that the curvature is large (α' reaching 2.0) for high τ_a cases and that the curvature averages about zero for τ_{a500} of ~0.2, with lower values of the second derivative at lower τ_a values. It is possible that the curvature of the opposite sign, seen for lower τ_a may be due to the presence of large biogenically produced particles. However, it is noted that at low τ_a values there may be significant errors in the determination of both α and the second derivative because of the previously mentioned uncertainties in τ_a of the order of 0.01-0.02. Uncertainties in τ_a of this magnitude result in small errors in α and the second derivative when τ_a values are high since these values are a small percentage of the aerosol optical depth, but these errors are very high when the τ_a values are themselves of a similar order of magnitude. The second derivative is particularly sensitive to uncertainty in τ_a at very low optical depth. For example, the 340, 675, and 1020 nm calibration coefficients and stability were less certain than the other wavelengths for the instrument at Los Fierros in 1998, resulting in larger uncertainty in computed τ_a at those wavelengths. As a result, inclusion of 675 nm τ_a data (in addition to 380, 440, 500, and 870 nm τ_a) in the computation of the second derivative for the Los Fierros data presented here in Figure 7b resulted in values of α' reaching a minimum of ~ -1.0 versus ~ -2.0 for the polynomial fit value without the 675 nm data for low aerosol optical depths (<0.2). However, the values of α' at larger τ_a are very similar for both sets of data, typically within ~0.10.

3.2. Urban/Industrial Aerosols

In the mid-Atlantic region of the United States during the summer months there are often periods of light to heavy aerosol loading as a result of the pollution emitted from various anthropogenic sources, such as industrial processes, electricity generation from fossil fuel combustion, and the combustion of fossil fuels from vehicular transportation. This pollution results in significant increases in aerosol optical depth [*Kaufman and Fraser*, 1983], and these aerosols have been found to be highly hygroscopic in nature [*Kotchenruther and Hobbs*, 1998]. We present data from τ_a measurements made

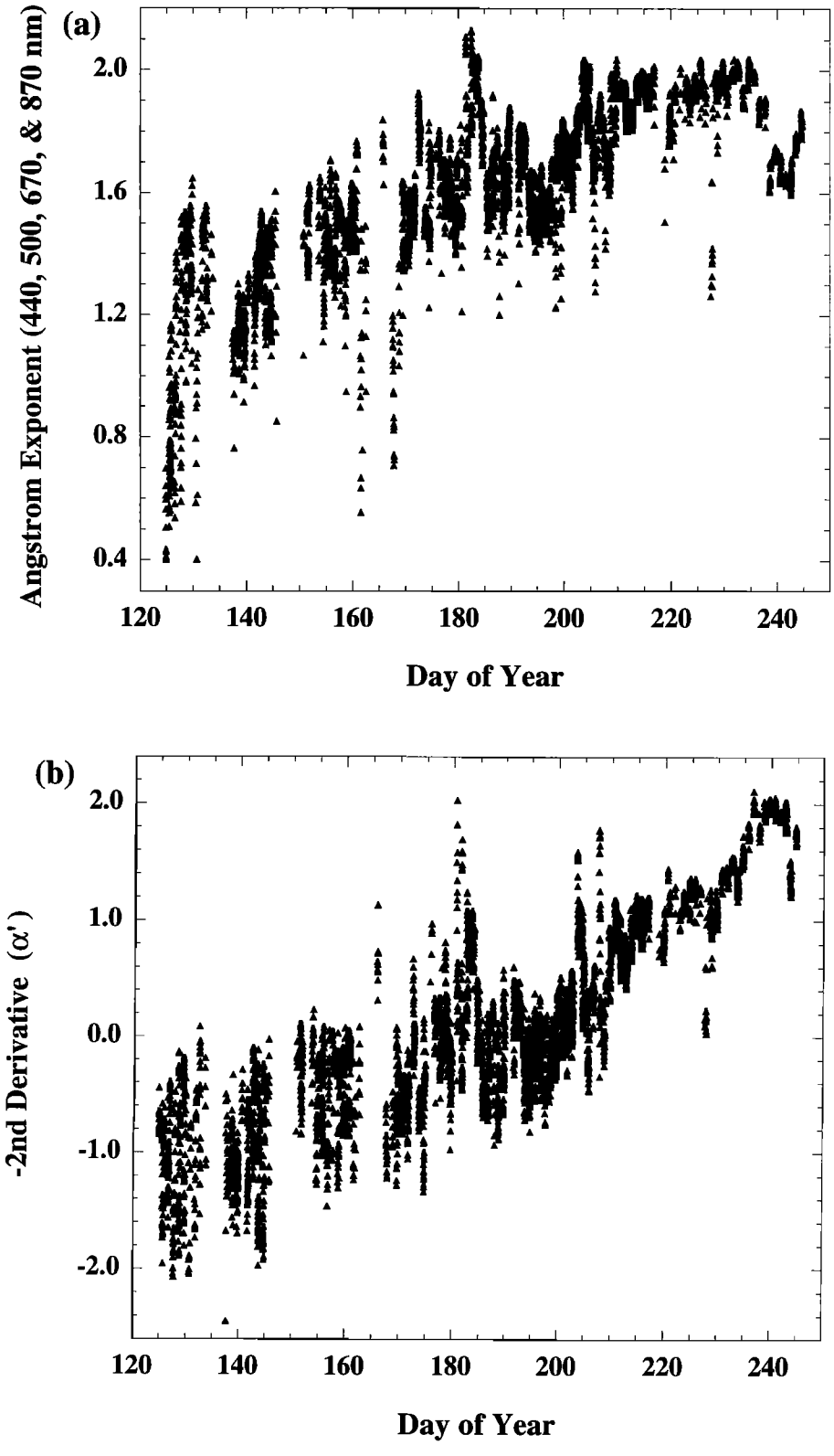

Figure 6. (a) The seasonal variation of the Angstrom wavelength exponent computed by linear regression of ln τ_a versus ln λ at 440, 500, 675, and 870 nm for Los Fierros, Bolivia from May 4 through September 1, 1998 (same site and time period as Figure 5). (b) Same as Figure 6a but for the negative of the second derivative of ln τ_a versus ln λ (α') computed from the second-order polynomial fit utilizing τ_a measurements made at 380, 440, 500, and 870 nm.

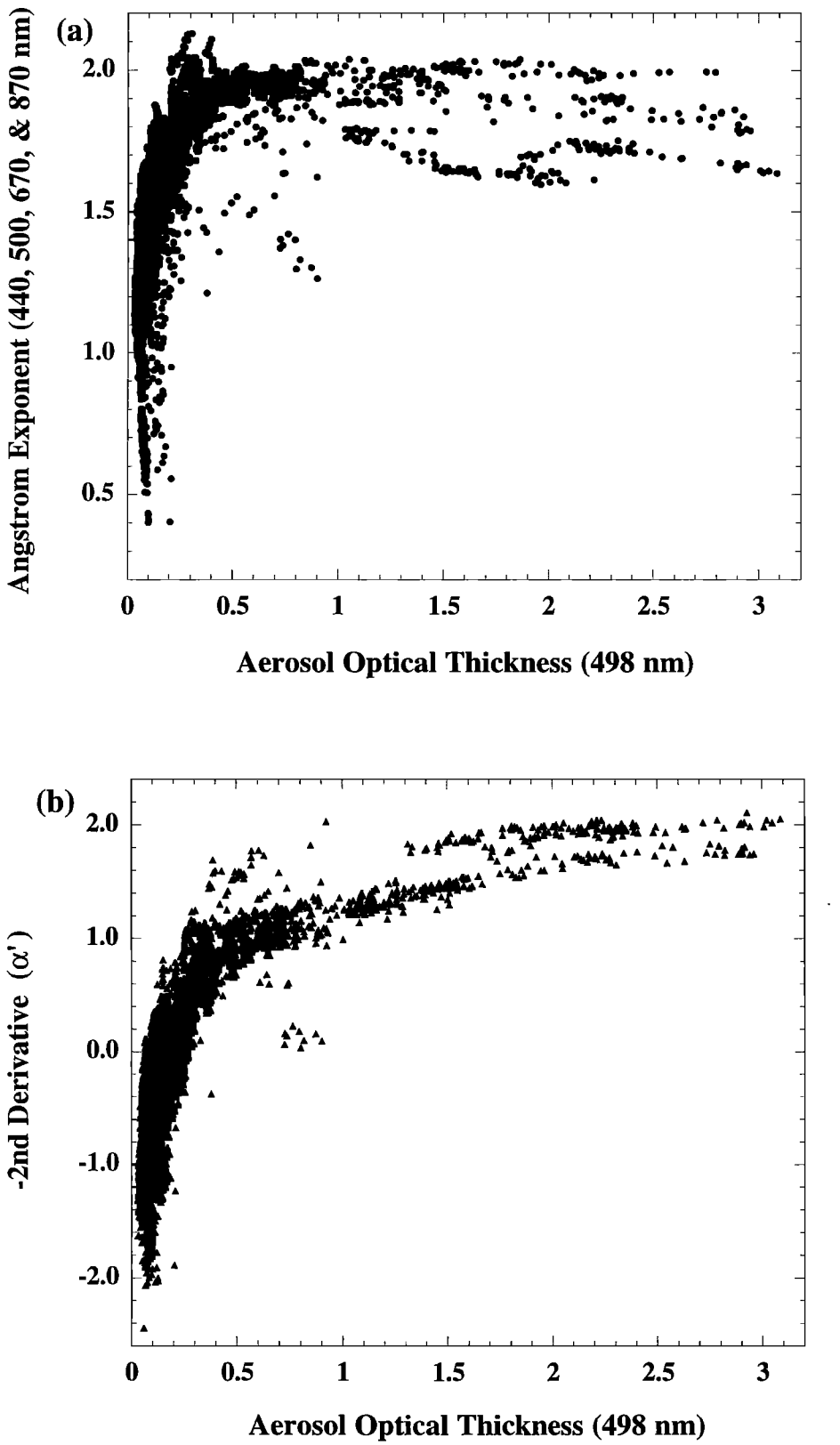

Figure 7. (a) The same Angstrom wavelength exponent data shown in Figure 6a but plotted versus the aerosol optical depth at 498 nm. (b) The same negative second derivative of ln τ_a versus ln λ (α') data as shown in Figure 6b, but plotted versus the aerosol optical depth at 498 nm.

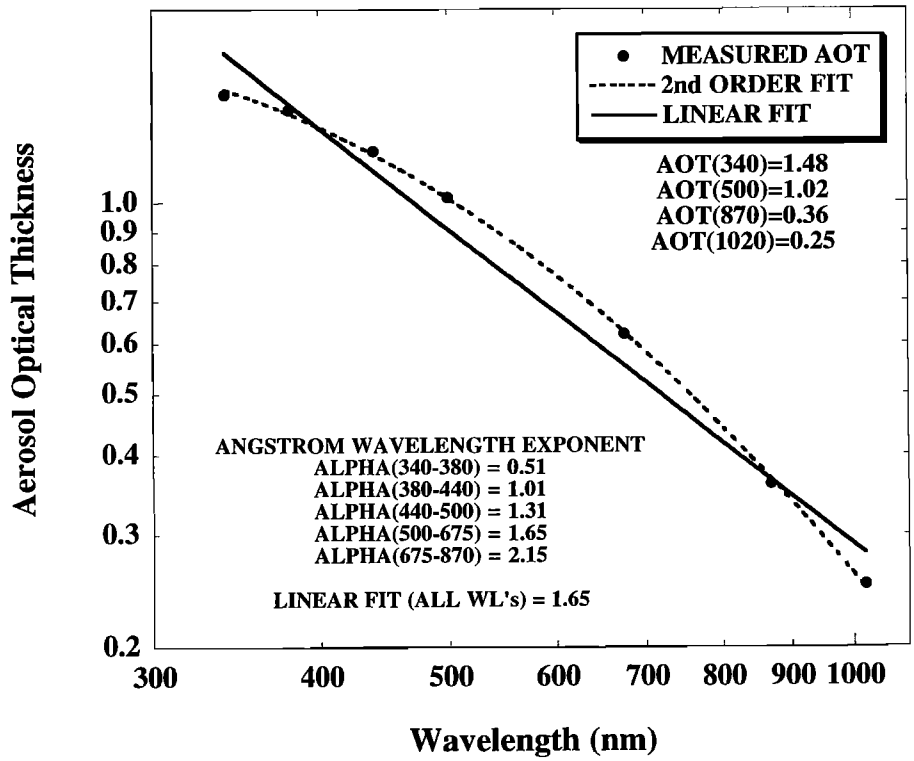

Figure 8. Same as Figure 1a, except for urban aerosols at Goddard Space Flight Center (GSFC) on July 15, 1997 at 1458 UT, when τ_{a500} = 1.02.

at GSFC in Greenbelt, Maryland (39°01'N, 76°52'W), which are affected by both locally generated pollution and aerosol pollution that has been advected from moderate to long distances from other urbanized regions in the eastern United States. Figure 8 shows data from a day with very high aerosol loading, July 15, 1997, at 1458 UT, when τ_{a500}=1.02. Similar to the case of biomass burning aerosols in South America and Africa, there is marked curvature in the ln τ_a versus ln λ relationship for urban pollution. The second-order polynomial fit to the measured τ_a is very good, with maximum differences of only 0.025 (at 340 nm), while the linear fit results in differences that range from -0.11 at 500 nm to 0.24 too high at 340 nm. It is noted that the instruments whose data we present for the GSFC cases were recently (within 2 months or less) calibrated at MLO, Hawaii, and therefore the uncertainty in τ_a for these data due to zero airmass voltage calibration uncertainty is only ~0.005 or less. The aerosol volume size distribution retrieved from almucantar sky radiance inversion for measurements made on this same day (~3 hours earlier) are shown in Figure 9. Similar to the size distribution for the August 24, 1998 data in Concepcion, Bolivia, for smoke aerosols (Figure 4), the accumulation mode aerosols dominate the volume size distribution, and the peak of this mode is about an order of magnitude greater than the peak of the coarse particle mode.

Also shown in Figure 9 are the size distribution retrievals from 2 other days of measurements at GSFC where τ_a is significantly lower than it was on July 15, 1997. As expected, the magnitude of the accumulation mode $dV/d(\ln r)$ decreased as τ_a decreases, and in addition, the accumulation mode peak radius decreased from ~0.21 μm at τ_{a500}=0.77 to ~0.11 μm at τ_{a500}=0.17. This is very similar to the change of the accumulation mode radius as a function of τ_a that was observed by *Remer and Kaufman* [1998], also for GSFC data, and which they primarily attribute to the the swelling of these hygroscopic aerosols from increased humidity and to cloud processing. It is interesting to note that the change in acccumulation mode radius as τ_a increases for biomass burning smoke (Figure 4) is much smaller than the increase in radius for urban aerosols, possibly in part because of the much lower humidification factors for biomass burning versus urban aerosols [*Kotchenruther and Hobbs*, 1998]. The values of α' for the three urban aerosol (GSFC) cases (Table 1) show a transition from a value of 1.76 (strong curvature) at τ_{a500}=1.02 to weak curvature in the opposite direction (-0.22) for τ_{a500}=0.17. This is the result of a decreasing dominance of the positive curvature accumulation mode as τ_a decreases and the increasing influence of the coarse mode particle optical effects.

It is noted that the urban aerosol optical characteristics presented here may only be representative of urban aerosols in the mid-Atlantic United States region. The processes that form the aerosols in other urban regions may differ. In addition, the fuels utilized in urban activity and industries, the environmental conditions of temperature, humidity, solar radiation intensity, altitude, cloud cover, and wind speed (all of which may affect aerosol production and evolution in time) range widely for various urban regions of the world.

3.3. Desert Dust Aerosols

In strong contrast to biomass burning and urban aerosols, which are dominated by fine mode accumulation particles, desert dust is dominated by coarse mode particles, composed of

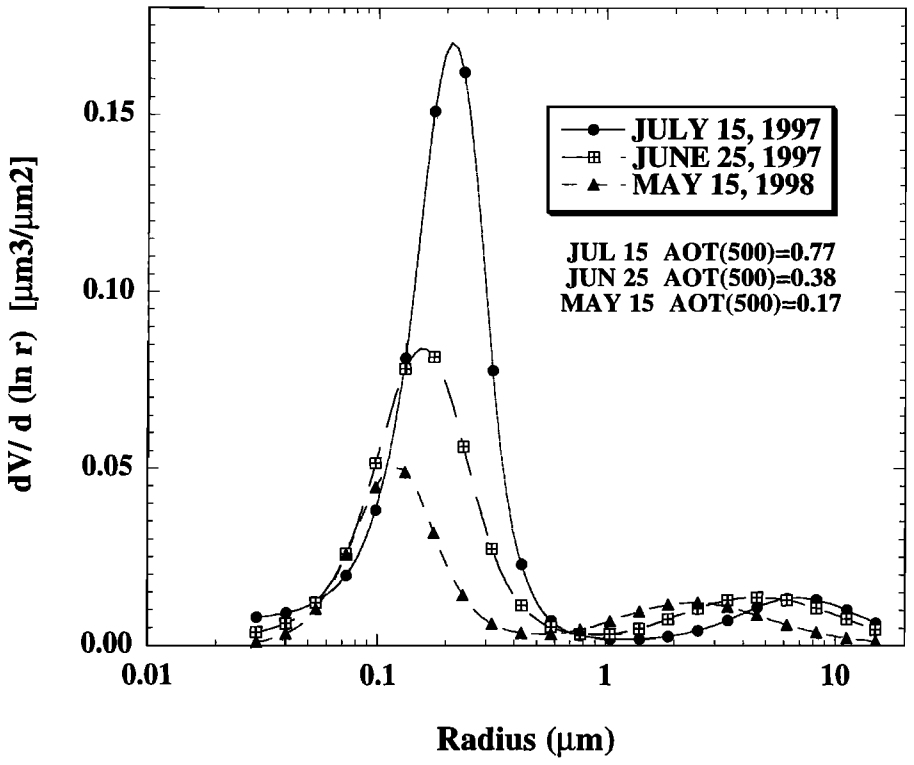

Figure 9. Aerosol volume size distributions for urban aerosols at GSFC for three days in 1997-1998 with different aerosol optical depths. The retrievals were derived from simultaneous analyses of sky radiances in the almucantar and spectral τ_a at 440, 675, 870, and 1020 nm with observations made at 1147 UT on July 15, 1997, at 1233 UT on June 25, and at 1241 UT on May 15, 1998.

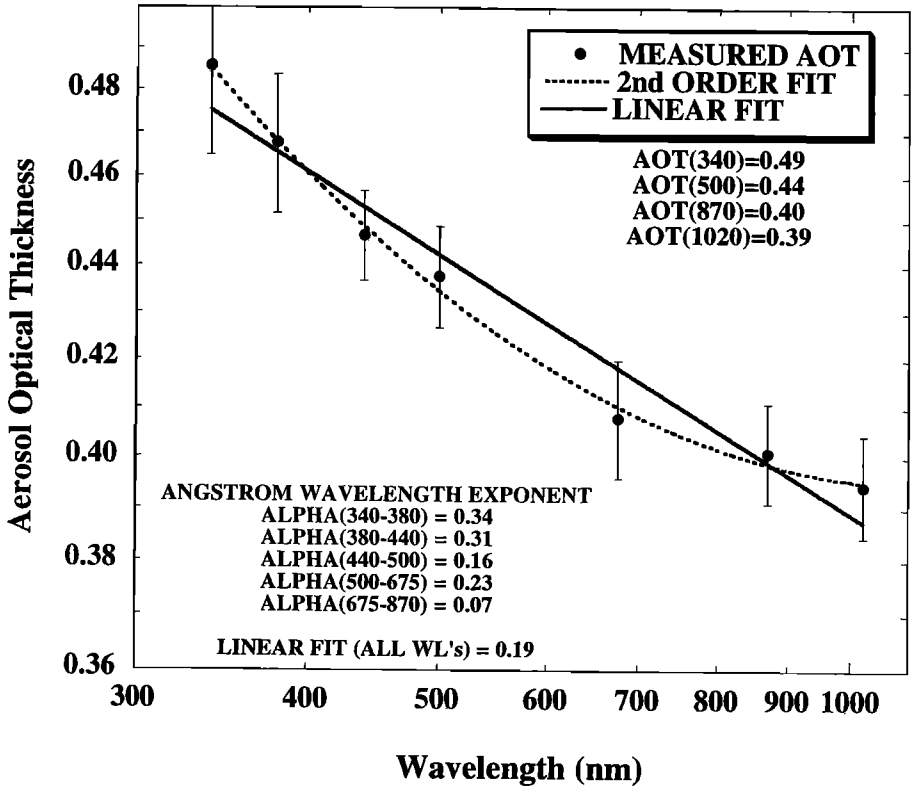

Figure 10. Same as Figure 1a, except for desert dust aerosols at Dalanzadgad, Mongolia on April 18, 1998, at 1008 UT, when $\tau_{a500} = 0.44$.

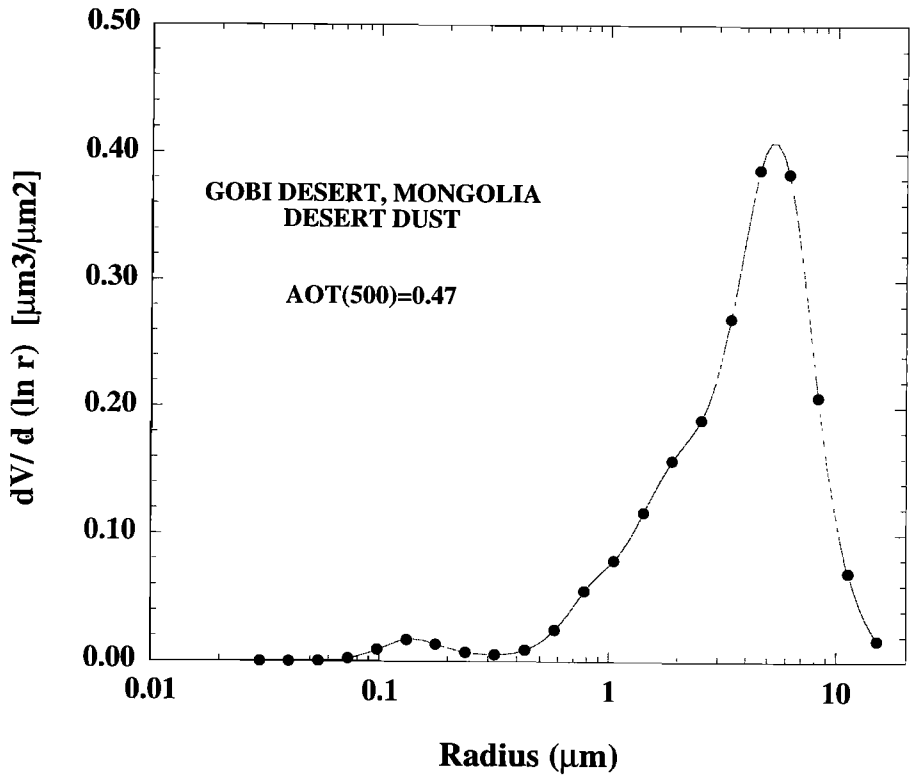

Figure 11. Aerosol volume size distribution for desert dust aerosols at Dalanzadgad, Mongolia for the same day as the data shown in Figure 10 but for 0955 UT.

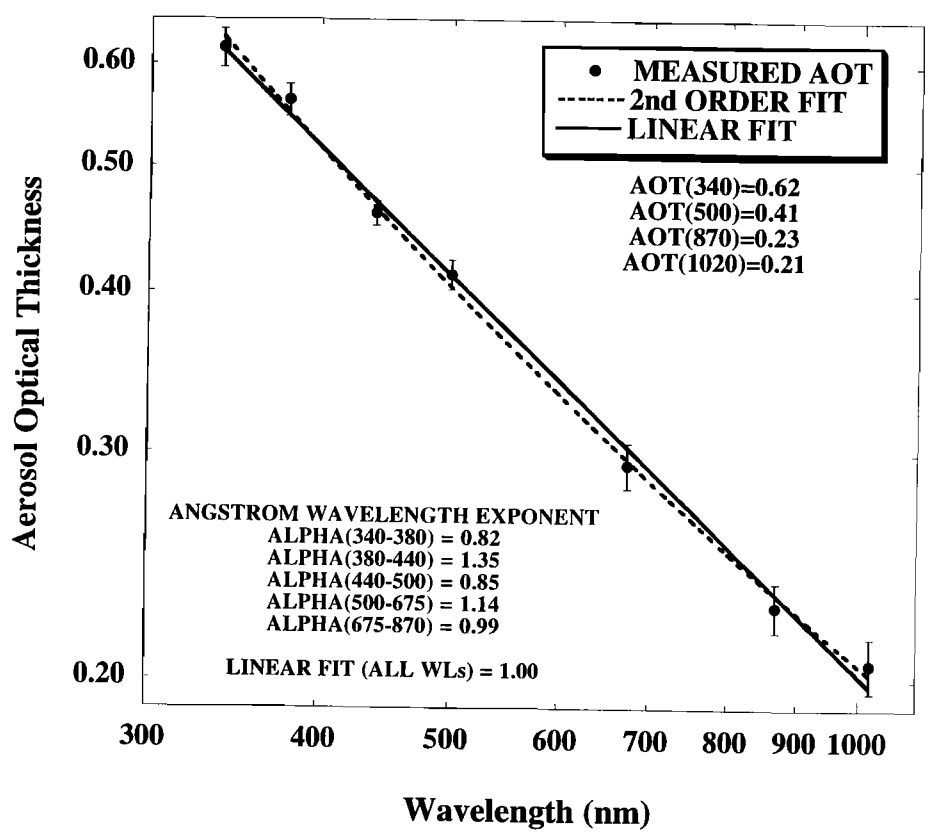

Figure 12. Same as Figure 1a, except for desert dust aerosols at Bahrain on August 5, 1998, at 1144 UT, when $\tau_{a500} = 0.41$.

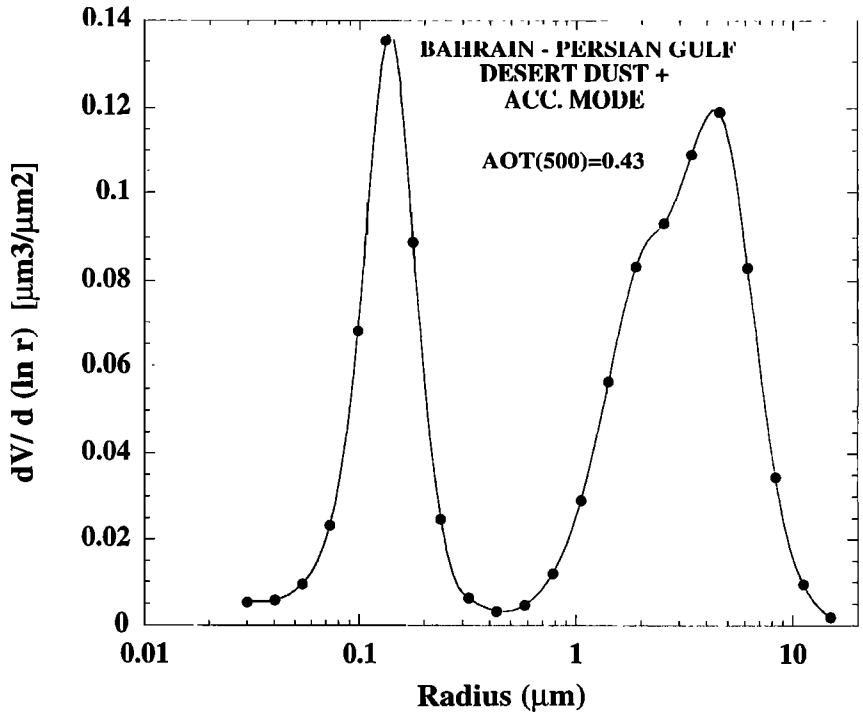

Figure 13. Aerosol volume size distribution for desert dust aerosols at Bahrain for the same day as the data shown in Figure 12 but for 1303 UT.

airborne desert soil material. The first case we consider is from AERONET measurements made in the Gobi desert at Dalanzadgad, Mongolia (43°34'N, 104°25'E) on April 18, 1998. This case was a part of a multiday desert dust event that resulted in long range transport of Gobi dust across the Pacific to North America. In Figure 10, there is some curvature in the ln τ_a versus ln λ relationship; however, the difference between both the linear fit and second-order polynomial fit and the measured τ_a values was 0.01 or less at all wavelengths. Therefore, since these differences are of the same order of magnitude as the uncertainty in τ_a measurement, there is no significant departure of the data from the linear relationship. The value of α for this case (computed from linear regression fit to all wavelengths) is 0.19, while α' is -0.20 (Table 1). The volume size distribution of the aerosols for this case is shown in Figure 11, with the dominant coarse-particle mode having a computed effective radius of 1.75 μm. As was mentioned previously, for particles of this size, there is only a 0.7% adjustment of measured τ_a required in order to account for the aerosol forward scattered radiance into the field of view of the sunphotometer [*Kinne*, 1997]. Therefore the correction of apparent τ_a to actual τ_a results in an increase of only ~0.003, which is insignificant given the magnitude of the other measurement uncertainties.

A second desert dust case that we present here is from measurements made in the Persian Gulf on the island of Bahrain (26°19'N, 50°30'E). Here there is no significant curvature to the ln τ_a versus ln λ relationship (Figure 12 and Table 1). The value of α for this case (computed from a linear regression fit to all wavelengths) is 1.00, while α' is -0.11. This value of α was typical for many days at this site in 1998. The much greater value of α for the Bahrain case versus the Mongolian dust case is due to the presence of a second dominant aerosol mode of accumulation-sized particles (Figure 13). The source of these accumulation mode particles in Bahrain is uncertain but may be the result of industrial sources and oil industry related activity in the region. However, the comparison of these two desert dust cases in Mongolia and Bahrain shows that there is very little curvature in the ln τ_a versus ln λ relationship when coarse mode aerosols are present in appreciable amounts and that the magnitude of α yields appreciable information about the relative magnitude of the optical effects of fine versus coarse particles.

Therefore, for the three major types of aerosols studied here (biomass burning, urban, and desert dust) we have shown that the presence of positive curvature in ln τ_a versus ln λ is indicative of the dominance of accumulation mode sized particles in the aerosol volume size distribution and that the addition of coarse particles to the size distribution results in a marked decrease in curvature. Since curvature in ln τ_a versus ln λ can be detected by a minimum of three wavelengths of τ_a retrievals, both satellite and ground-based retrievals in three or more wavelengths have the potential to yield significantly more information about particle size distributions than two wavelength retrievals. With the advent of measurements from the MODIS and Multiangle Imaging Spectroradiometer (MISER) instruments on the Terra and EOS-PM satellite platforms planned to start in 1999 it may be possible to retrieve τ_a in three of more wavelengths over ocean surfaces where the spectral surface reflectance magnitudes are sufficiently well known.

4. Summary and Conclusions

The wavelength dependence of τ_a was investigated over the range of 340 to 1020 nm utilizing ground-based direct solar measurements from AERONET radiometers for biomass burning, urban, and desert dust aerosols. Biomass burning and

urban aerosols exhibit pronounced curvature in the ln τ_a versus ln λ relationship at moderate to high optical depths because of the dominance of the accumulation mode sized particles in the aerosol size distribution. A second-order polynomial fit to the measured τ_a values (340-1020 nm) gives excellent agreement with differences of the same order as the measurement uncertainty of τ_a (~0.01-0.02). A linear Angstrom exponent type of fit, however, results in significant differences with the measurements (as high as 0.57 at 340 nm for a biomass burning case where τ_{a340} =3.02). This curvature of ln τ_a versus ln λ results in spectral variations of α that are as large as a factor of 3-5 from 340 to 870 nm for high optical depth accumulation mode dominated aerosols. We suggest that α' (equation (8)) be utilized to quantify the amount of curvature (and thus the relative influence of accumulation versus coarse mode particles) and that this parameter be utilized in conjunction with α to characterize more fully the wavelength dependence of τ_a. For aerosol size distributions with a significant coarse mode (such as desert dust), there is very little curvature in ln τ_a versus ln λ, and the value of α itself provides useful information on the relative influence of coarse versus accumulation mode aerosols. This relative optical influence between modes also applies to the case for low optical depth urban and biomass burning aerosols.

Comparison of α values from satellite retrievals and surface-based techniques therefore need to take into account the spectral range of the observations since our data show that α varies substantially as a function of wavelength for accumulation mode dominated aerosols. In addition, if satellite retrievals of τ_a can be made for three or more wavelengths, as may be the case for ocean retrievals with future MODIS and MISR instrument data, then the measure of the curvature in ln τ_a versus ln λ may yield additional information on the aerosol size distributions. Also, in order to obtain accurate estimates of τ_a within spectral regions where gaseous absorption is strong or where there are typically very few measurements available, it is important to use a second-order fit to the data to account for the curvature in ln τ_a versus ln λ. Examples of these types of cases are in the computation of τ_a at UVB wavelengths (290-320 nm) for studies of the aerosol effects on UVB fluxes and at near infrared wavelengths (>1100 nm) for use in remote sensing applications and energy balance calculations.

Acknowledgments. This project was supported by Mike King, EOS Project Office. We acknowledge the critical efforts of Nader Abuhassen and Wayne Newcomb in maintaining and adjusting the radiometers deployed in the AERONET network. We thank Chuck McClain, for providing the data from the Bahrain site utilized in this study. We also thank site managers in Bolivia, Tim Killeen (Missouri Botanical Gardens) and Ademar Soto; the Mongu, Zambia site manager, Mukufute Mukulabai (Zambian Meteorological Service); the Bahrain site managers CDR Heishman (U.S. Navy 5th Fleet) and Andreas Goroch (Naval Research Lab); and the Dalanzadgad, Mongolia, site managers, Dashjamtsyn Zorig,Chairman, Mr. Enkhtuwshin, and Mr. Surenjaw. We also thank the reviewers for their thoughtful comments and suggestions, which helped in improving the manuscript.

References

Angstrom, A., On the atmospheric transmission of Sun radiation and on dust in the air, *Geogr. Ann., 12*, 130-159, 1929.

Artaxo, P., H. Storms, F. Bruynseels, R. Van Grieken, and W Maenhaut, Composition and sources of aerosols from the Amazon Basin, *J. Geophys. Res., 93*, 1605-1615, 1988.

Artaxo, P., et al., Aerosol properties in the central Amazon Basin wet season during the LBA/CLAIRE experiment, *Eos Trans. AGU, 79*(45), Fall Meet. Suppl., F155, 1998.

Box, M. A., and A. Deepak, Atmospheric scattering corrections to solar radiometery, *Appl. Opt., 18*, 1941-1949, 1979.

D'Almeida, G. A., On the variability of desert aerosol radiative characteristics, *J. Geophys. Res., 92*, 3017-3026, 1987.

Dubovik, O., B. N. Holben, M. D. King, A. Smirnov, T. F. Eck, S. Kinne, and I. Slutsker, A flexible inversion algorithm for retrieval of aerosol optical properties from sun and sky radiance measurements, paper presented at ALPS '99, Cent. Natl. d'Etudes Spatiales, Meribel, France, January 18-22, 1999.

Eck, T. F., B. N. Holben, I. Slutsker, and A. Setzer, Measurements of irradiance attenuation and estimation of aerosol single scattering albedo for biomass burning aerosols in Amazonia, *J. Geophys. Res., 103*, 31,865-31,878, 1998.

Elden, B., The refractive index of air, *Meteorology, 2*, 71-80, 1966.

Halthore, R. N., S. E. Schwartz, J. J. Michalsky, G. P. Anderson, R. A. Ferrare, B. N. Holben, and H. M. Ten Brink, Comparison of model estimated and measured direct-normal solar irradiance, *J. Geophys. Res., 102*, 29,991-30,002, 1997.

Hansen, J. E., and L. D. Travis, Light scattering in planetary atmospheres, *Space Sci. Rev., 16*, 527-610, 1974

Holben, B. N., T. F. Eck, and R. S. Fraser, Temporal and spatial variability of aerosol optical depth in the Sahel region in relation to vegetation remote sensing, *Int. J. Remote Sens., 12*, 1147-1163, 1991.

Holben, B. N., A. Setzer, T. F. Eck, A. Pereira, and I. Slutsker, Effect of dry season biomass burning on Amazon basin aerosol concentrations and optical properties, *J. Geophys. Res., 101*, 19,465-19,481, 1996.

Holben, B. N., et al., AERONET - A federated instrument network and data archive for aerosol characterization, *Remote Sens. Environ., 66*, 1-16, 1998.

Hoppel, W. A., J. W. Fitzgerald, G. M. Frick, R. E. Larson, and E. J. Mack, Aerosol size distributions and optical properties found in the marine boundary layer over the Atlantic Ocean, *J. Geophys. Res., 95*, 3659-3686, 1990.

Junge, C. E., The size distribution and aging of natural aerosols as determined from electrical and optical measurements in the atmosphere, *J. Meteorol., 12*, 13-25, 1955.

Kaufman, Y. J., Aerosol optical thickness and atmospheric path radiance, *J. Geophys. Res., 98*, 2677-2692, 1993.

Kaufman, Y. J., and R. S. Fraser, Light extinction by aerosols during summer air pollution, *J. Clim. Appl. Meteorol., 22*, 1694-1706, 1983.

Kaufman, Y. J., A. Setzer, D. Ward, D. Tanre, B. N. Holben, P. Menzel, M. C. Pereira, and R. Rasmussen, Biomass burning airborne and spaceborne experiment in the Amazonas (BASE-A), *J. Geophys. Res., 97*, 14,581-14,599, 1992.

Kaufman, Y. J., D. Tanre, A. Karnieli, L. Remer, and B. N. Holben, Aerosol absorption and measurements from combination of Landsat data and CIMEL Sun/sky radiometers, paper presented at ALPS '99, Cent. Natl. d'Etudes Spatiales, Meribel, France, January 18-22, 1999.

Kavouras, I. G., N. Mihalopoulos, and E. Stephanou, Formation of atmospheric particles from organic acids produced by forests, *Nature, 395*, 683-686, 1998.

King, M. D., and D. M. Byrne, A method for inferring total ozone content from spectral variation of total optical depth obtained with a solar radiometer, *J. Atmos. Sci., 33*, 2242-2251, 1976.

Kinne, S., T. P. Ackerman, M. Shiobara, A. Uchiyama, A. J. Heymsfield, L. Miloshevich, J. Wendell, E. W. Eloranta, C. Purgold, and R. W. Bergstrom, Cirrus cloud radiative and microphysical properties from ground observations and in situ measurements during FIRE 1991 and their application to exhibit problems in cirrus solar radiative transfer modeling, *J. Atmos. Sci., 54*, 2320-2344, 1997.

Kotchenruther, R., and P. V. Hobbs, Humidification factors of aerosols from biomass burning in Brazil, *J. Geophys. Res., 103*, 32,081-32090, 1998.

Li, Y., T. H. Demetriades-Shah, E. T. Kanemasu, J. K. Shultis, and M. B. Kirkam, Use of second derivatives of canopy reflectance for monitoring prairie vegetation over different soil backgrounds, *Remote Sens. Environ., 44*, 81-87, 1993.

London, J., R. D. Bojkov, S. Oltmans, and J. I. Kelly, Atlas of the global distribution of total ozone July 1957-June 1967, *NCAR Tech. Note 133+STR*, 276 pp., Natl. Cent. for Atmos. Res., Boulder, Colo., 1976.

Martins, J. V., P. V. Hobbs, R. E. Weiss, and P. Artaxo, Sphericity and morphology of smoke particles from biomass burning in Brazil, *J. Geophys. Res., 103*, 32,051-32,057, 1998.

Nakajima, T., and A. Higurashi, A use of two-channel radiances for an aerosol characterization from space, *Geophys. Res. Lett., 25*, 3815-3818, 1998.

O'Neill, N., and A. Royer, Extraction of bimodal aerosol-size distribution radii from spectral and angular slope (Angstrom) coefficients, *Appl. Opt., 32*, 1642-1645, 1993.

Penndorf, R., Tables of the refractive index for standard air and the Rayleigh scattering coefficient for the spectral region between 0.2 and 20.0 microns and their application to atmospheric optics. *J. Opt. Soc. Am., 47*, 176-182, 1957.

Prins, E.M., and W.P. Menzel, Trends in South American biomass burning detected with the GOES visible infrared spin scan radiometer atmospheric sounder from 1983 to 1991, *J. Geophys. Res., 99*, 16,719-16,735, 1994.

Prins, E. M., J. M. Feltz, W. P. Menzel, and D. E. Ward, An overview of GOES-8 diurnal fire and smoke results for SCAR-B and 1995 fire season in South America, *J. Geophys. Res., 103*, 31,821-31,835, 1998.

Reid, J. S., and P. V. Hobbs, Physical and optical properties of young smoke from individual biomass fires in Brazil, *J. Geophys. Res., 103*, 32,013-32,031, 1998.

Reid, J. S., P. V. Hobbs, R. J. Ferek, D. R. Blake, J. V. Martins, M. R. Dunlap, and C. Liousse, Physical, chemical, and optical properties of regional hazes dominated by smoke in Brazil, *J. Geophys. Res., 103*, 32,059-32,080, 1998.

Reid, J. S., T. F. Eck, S. A. Christopher, P. V. Hobbs, and B. N. Holben, Use of the Angstrom exponent to estimate the variability of optical and physical properties of aging smoke particles in Brazil, *J. Geophys. Res.*, in press, 1999.

Remer, L. A. and Y. J. Kaufman, Dynamic aerosol model: Urban/industrial aerosol, *J. Geophys. Res 103*, 13859-13871, 1998.

Remer, L. A., Y. J. Kaufman, B. N. Holben, A. M. Thompson, and D. P. McNamara, Biomass burning aerosol size distribution and modeled optical properties, *J. Geophys. Res., 103*, 31,879-31,891, 1998.

Russell, P. B., et al., Pinatubo and pre-Pinatubo optical depth spectra: Mauna Loa measurements, comparisons, inferred particle size distributions, radiative effects, and relationship to lidar data, *J. Geophys. Res., 98*, 22,969-22,985, 1993.

Schmid, B., J. Michalsky, R. Halthore, M. Beauharnois, L. Harrison, J. Livingston, P. Russell, B. Holben, T. Eck, and A. Smirnov, Comparison of aerosol optical depth from four solar radiometers during the Fall 1997 ARM intensive observation period, *Geophys. Res. Lett., 26*, 2725-2728, 1999.

Shaw, G. E., Sun photometry, *Bull. Am. Meteorol. Soc., 64*, 4-10, 1983.

Tegen, I., and A. A. Lacis, Modeling of particle size distribution and its influence on the radiative properties of mineral dust aerosol, *J. Geophys. Res., 101*, 19,237-19,244, 1996.

Young, A. T., Revised depolarization corrections for atmospheric extinction, *Appl. Opt., 19*, 3427-3428, 1980.

O. Dubovik, I. Slutsker, and A. Smirnov, Science Systems and Applications, Inc., Code 923, NASA Goddard Space Flight Center. Greenbelt, MD 20771. (dubovik@spamer.gsfc.nasa.gov, asmirnov@spamer.gsfc.nasa.gov, ilya@spamer.gsfc.nasa.gov)

T. F. Eck, Raytheon ITSS, Code 923, NASA Goddard Space Flight Center. Greenbelt, MD 20771. (tom@spamer.gsfc.nasa.gov)

B. N. Holben, Biospheric Sciences Branch, Code 923, NASA Goddard Space Flight Center. Greenbelt, MD 20771. (brent@spamer.gsfc.nasa.gov)

S. Kinne, University of Maryland, Baltimore, Code 923, NASA Goddard Space Flight Center. Greenbelt, MD 20771. (kinne@spamer.gsfc.nasa.gov)

N. T. O'Neill, NRC, Code 923, NASA Goddard Space Flight Center. Greenbelt, MD 20771. (norm@spamer.gsfc.nasa.gov)

J. S. Reid, SPAWARSYSCEN SAN DIEGO D883, 49170 Propagation Path, San Diego, CA, 92152-7385. (jreid@spawar.navy.mil)

(Received May 11, 1999; revised August 10, 1999;
accepted August 18, 1999.)